Maglad *et al. Int J Concr Struct Mater (2023)17:49*
https://doi.org/10.1186/s40069-023-00617-0

International Journal of Concrete Structures and Materials

RESEARCH

Open Access

Experimental Study of the Flexural Behaviour of RC Beams Made of Eco-friendly Sawdust Concrete and Strengthened by a Wooden Plate

Ahmed M. Maglad[1], Walid Mansour[2*], Sabry Fayed[2], Bassam A. Tayeh[3], Ahmed M. Yosri[4] and M. Hamad[4]

Abstract

In this paper, the effectiveness of the strengthening by a wooden plate for reinforced concrete (RC) beams that incorporate waste sawdust (SD) as a partial substitute for fine aggregate (sand) has been investigated. To this end, two types of concrete mixtures were made: normal concrete (NC) and sawdust concrete (SDC), which was made by substituting 15% of the volume of sand with SD. Five RC beams (100 mm in depth, 200 mm in width, and 1500 mm in length) were experimentally tested for flexural behavior under four-point loading. Three strengthening schemes were used in this study. The first scheme used a wooden plate that was only fixed by an adhesive layer. The second and third schemes were applied by a wooden plate, which was fixed by an adhesive layer and steel angles (two and eleven angles). The findings of the study indicate that although the concrete's workability, compressive, and splitting tensile strengths were reduced with the addition of SD, the ultimate load of the beam with SD was lower than that of the control beam, with a slight variation of approximately 4%. Moreover, strengthening the RC beam with a wooden plate and two steel angles yielded the highest load capacity among all tested beams, 20% higher than the control specimen. The study's findings offered useful information for developing eco-friendly sawdust concrete beams with efficient strengthening techniques for potential future uses.

Keywords Sawdust, Wood recycling, Wooden plate, Strengthening, RC beams, Flexural strength, Mechanical properties, Partial sand replacement

1 Introduction

The global construction industry is expanding quickly, and as a result, more raw materials are being consumed for concrete manufacture, which has resulted in the depletion of numerous non-renewable materials (Habert et al., 2010; Khan et al., 2020). One potential remedy for environmental pollution and energy sustainability is the production of green energy (Wasim et al., 2022). Researchers are focusing on the use of agricultural and industrial waste in concrete mixtures for the sustainable development of the building sector as a result of the primary concerns of resource depletion and rising global pollution. As supplementary cementitious materials, industrial wastes like fly ash (Elsayed et al., 2022), silica fume (Amin et al., 2022), and agricultural wastes like rice husk ash (Faried et al., 2021), eggshell (Hamada et al., 2020), olive waste ash (Hakeem et al., 2022), corncob ash (Ahmed & Kamau, 2017), and palm oil fuel ash (Zeyad et al., 2019) are already used in concrete mixtures. Moreover, other waste materials, such as rubber (Alshaikh et al., 2022), wood waste (Siddique et al., 2020),

Journal information: ISSN 1976-0485 / eISSN 2234-1315.

*Correspondence:
Walid Mansour
waled_mansour@eng.kfs.edu.eg
[1] Department of Civil Engineering, Najran University, Najran, Saudi Arabia
[2] Civil Engineering Department, Faculty of Engineering, Kafrelsheikh University, Kafrelsheikh 33511, Egypt
[3] Civil Engineering Department, Faculty of Engineering, Islamic University of Gaza, Gaza, Palestine
[4] Civil Engineering Department, Faculty of Engineering, Delta University for Science and Technology, Belkas, Egypt

volcanic pumice powder (Abdullah et al., 2022), and construction debris (Patra et al., 2022), are being considered cheap and plentiful alternatives. The waste material produced by the wood-based industry is called sawdust (SD). It develops as small, uneven wood chips or small wood debris as a result of the slicing of timber logs into various sizes. The SD sizes are influenced by the wood types and saw tooth sizes. Worldwide, enormous amounts of SD are produced each year. The 3 million tons of SD produced annually in the USA are generally discarded in landfills (Butt et al., 2016; Cheah & Ramli, 2013). The environment is endangered by the disposal of SD on open ground (Mangi et al., 2017). Researchers believe that SD can be used as a raw material for the production of fine boards, particle boards, etc., or as a source of energy. Currently, SD is utilized in the production of cement-based products (e.g., cement-bonded particle boards). Both types of aggregates are key ingredients in concrete mixtures, and as demand grows within the construction sector, natural aggregate supplies are being rapidly depleted. Around the world, each year, natural aggregates are taken from crushed rock, riverbeds, lakes, and various resources in amounts close to eleven billion tons (Batool et al., 2021). To reduce the damaging impacts on the environment, numerous nations have put restrictions on the extraction of sand from rivers in recent years (Alwesabi et al., 2020; Shahria Alam et al., 2013; Ulloa et al., 2013). Researchers are looking into using SD as a partial substitute for fine aggregate (i.e., sand) in the production of mortar due to the compatibility between wood and cement (Siddique et al., 2020). Siddique et al. (2020) reported a substantial decrease in the hardened properties as well as the workability by increasing the SD ratio in concrete and replacing fine aggregates with it. Similar results were observed by Ahmed et al. (2018), Oyedepo et al. (2014), Vaidkelionis and Vaickelionene (2006), and Foti and Cavallo (2018). However, SD ash has been used successfully in place of sand in concrete mixtures, according to Mageswar and Vidivelli (2009). According to previous research, SD may be a practical choice to use as a raw material for the production of sustainable and lightweight concrete products. The mechanical properties of concrete are negatively impacted by the inclusion of SD; however, previous research has shown that it has a lot of potential as a substitute aggregate in low-to-medium strength concrete applications, such as partition walls, pipe bedding, sidewalks, concrete blocks, roadside barriers on highways and bridges, reduced strength footings, and low-risk applications. For the construction of low-rise concrete buildings involving the casting of roofs, 20 MPa concrete is employed in many African and Asian nations (such as Egypt, Libya, Pakistan, etc.). Recycled concrete with compressive strengths between 18 and 45 MPa is already permitted for use in structural and non-structural applications in Japan (Batool et al., 2021). A comprehensive investigation is therefore warranted to support the use of SD as a substitute for fine aggregate. Various strengthening schemes were also developed by researchers to increase the flexural capacity of RC beams. The RC jacketing technique is a frequent repair and rehabilitation procedure because it has the potential to increase stiffness and load capacity. This process has a number of disadvantages, though, including higher labor demands and longer construction times, as well as an increase in the final dimensions of repaired RC members, which may have an impact on the structure's dynamic properties (Altun, 2004). This resulted in the development of substitutes for the jacketing technique, including ferrocement, fiber-reinforced polymers (FRPs) (Zapris et al., 2023), carbon fiber-reinforced polymers (CFRP) (Aksoylu, 2022), fiber-reinforced mortar, the near surface mounted (NSM) technique (Jeevan et al., 2023), and ultra-high-performance concrete (UHPC) (Abadel et al., 2022). According to the literature, the majority of experimental research was carried out and concentrated on high-cost or difficult-to-implement materials, such as the jacketing technique, FRPs, CFRP, NSM, and UHPC, as strengthening schemes for the flexural capacity of RC beams. Contrarily, there is a lack of pertinent information regarding simultaneous easy and economic solutions (e.g., wooden plates), and all research has not taken into account the impact of wooden plates used as strengthening schemes and their use in improving the flexural capacity of RC beams. The feasibility of using SD effectively as a substitute for sand in RC beams, as well as wooden plates as a strengthening scheme has not been investigated yet. To address this gap, two types of concrete mixtures were made: normal concrete (NC) and sawdust concrete (SDC), which was made by substituting 15% of the volume of sand with SD. Five RC beams (100 mm in depth, 200 mm in width, and 1500 mm in length) were experimentally tested for flexural behavior under four-point loading. Three strengthening schemes were used in this study. The first scheme used a wooden plate that was only fixed by an adhesive layer. The second and third schemes were applied by a wooden plate, which was fixed by an adhesive layer and steel angles (two and eleven angles).

2 Experimental Program

2.1 Materials

The concrete mixtures in this investigation were made using ordinary Portland cement (OPC), aggregate, and sawdust.

Table 1 The chemical characteristics of OPC used in this study

Item	CaO	SiO_2	Al_2O_3	$CaSO_4$	Fe_2O_3	MgO	Sulphur	Alcalies	Total (%)
Percentage (%)	62	22	5	4	3	2	1	1	100

Fig. 1 SD sample

Table 2 The physical characteristics of SD used in this study

Properties	SD	Fine aggregate (sand)
Average particle size	500 µm	4.95 mm
Fineness Modulus	5.01	7.26
Specific gravity	2.12	2.50
Bulk density	421.5 kg/m^3	1302 kg/m^3
Water absorption	19.5%	0.8%

2.1.1 Cement

The ACI Mix Design (ACI, 2002) was used to design the control mixture, which had a cylinder compressive strength of 40 MPa at the age of 28 days. OPC of type 1 with a specific gravity of 3.15 has been used in the present research work in accordance with ASTM C150 (ASTM, 2007). Table 1 displays the chemical characteristics of cement.

2.1.2 Sawdust and Wooden Plates

In the timber industry, SD is a solid waste product resulting from wood's mechanical processing, which includes cutting, drilling, grinding, and scraping. As indicated in Fig. 1, a sample of SD was obtained from a nearby local wood workshop and used in the preparation of the concrete mixtures without any kind of treatment. SD samples were subjected to laboratory examinations to evaluate various physical characteristics with respect to the fine aggregate, which are summarized in Table 2. Fig. 2 displays the sieve analysis results for the SD particle size. Furthermore, the strengthening plates were made of beech wood and had the same compressive and tensile resistance of 45 MPa.

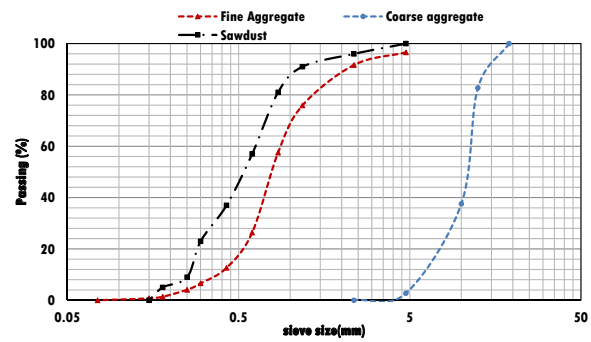

Fig. 2 Sieve analysis of SD, coarse, and fine aggregates

2.1.3 Aggregate

The fine aggregate (FA) was derived from natural sand and has the following specifications: 2.5 specific gravity, 7.26 fineness modulus, 0.8% water absorption rate, and 2.0% moisture content. The fine aggregate's maximum particle size was 4.95 mm. The coarse aggregate (CA) was derived from crushed dolomite and has the following specifications: 2.67 specific gravity, 1234 kg/m^3 bulk density, and a 0.8% water absorption rate. The coarse aggregate's maximum particle size was 19 mm. Sand and coarse gravel complied with the requirements of ASTM C33 (ASTM, 2016). The sieve analysis of the coarse as well as fine aggregates is presented in Fig. 2. The CA and FA gradients corresponded to ASTM C33 (ASTM, 2018).

2.1.4 Reinforcing Steel Rebars

In this investigation, deformed reinforcing steel rebars were employed. The diameters of the reinforcing rebars in metric units for the shear reinforcement were 8 mm (Ø8 mm), while for beam reinforcements they were 8 mm (Ø8 mm) at the top and 10 mm (Ø10 mm) at the bottom. According to ASTM-E8 (ASTM, 2009), Table 3 gives the ultimate and yield stresses for each of the reinforcing rebars under tensile test for an average of three segments, each measuring 600 mm in length.

Table 3 Properties of reinforcing rebar used in this study

Properties	Diameter of rebar	
	Ø8 mm	Ø10 mm
Yield stress (σ_y)	240 MPa	520 MPa
Strain at yield stress (ε_y)	1.2‰	2.25‰
Ultimate stress (σ_u)	380 MPa	620 MPa
Strain at ultimate stress (ε_u)	22‰	20‰

2.2 Specimen Preparation and Instrumentation

Sawdust concrete (SDC) and normal concrete (NC) were the two concrete mixtures employed. 15% of the volume of the fine aggregate (sand) was replaced by the sawdust in the SDC mixture. Replacing 15% of the sand ensures the elimination of sufficient weight from sawdust inside the concrete mixture, which is one of the most important objectives of the current research. In addition to the fact that the characteristics of RC beams are not significantly affected compared to the higher proportions, restoration of the ultimate capacity of the conventional beam can be obtained by strengthening with wooden plates. The water-to-cement ratio (0.6) was constant in each mixture. Table 4 provides a summary of the proportions of the concrete mixture. Almost two minutes were spent mixing the coarse and fine aggregates. SD was combined with both coarse and fine aggregates to create the SDC mixture. The following stage involves adding cement. For a further two minutes, the components were dry-mixed. Two phases of water addition (i.e., 70% and 30%) were made in the mixer, and each stage of mixing took about two minutes until the mixture was entirely homogeneous. Slump tests were immediately undertaken after the mixing procedure was finished. Then, using a vibrator, concrete was poured into the specimen molds. According to ACI 308R-01 R08 (ACI, 2008), the specimens were kept in lab conditions for 24 h. These specimens were eventually taken out of their molds. After that, the specimens were moist-cured for 28 days. The measurement tools are shown in Fig. 3. Two PI displacement transducers were used to measure strains in concrete surfaces, which were fixed by being glued at the top and bottom surfaces in the middle of the beam, as shown in Fig. 3. Also, another PI displacement transducer was fixed to the wooden strengthening plate. The mid-span beam's deflections were recorded with the use of a linear variable differential transformer (LVDT). According to all current measures and the available financial resources, experimental tests were carried out.

Table 4 Concrete mixtures' properties

Specimen ID	Unit	Water	Cement	Aggregate		SD
				Coarse	Fine	
NC	Weight (kg)	240	400	1300	650	0
SDC	Weight (kg)	240	400	1300	552.5	10.9

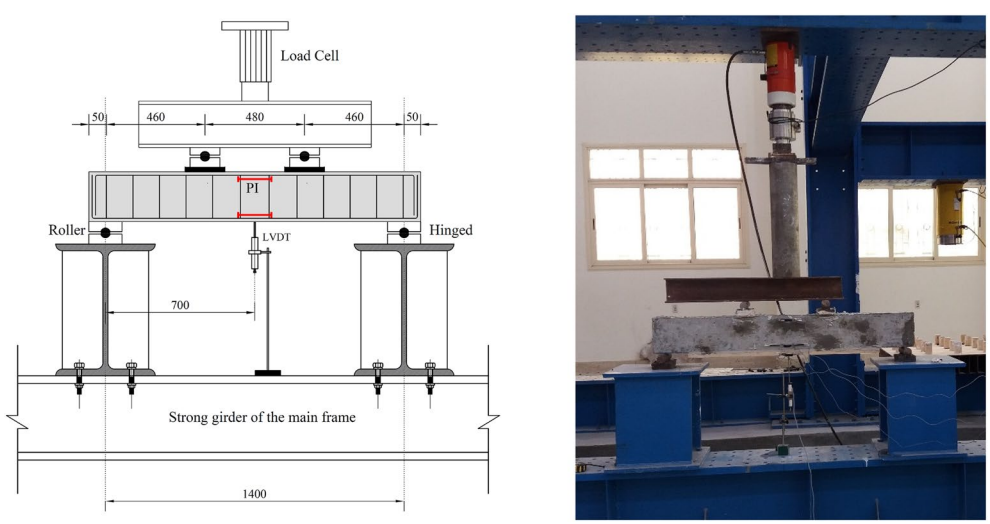

Fig. 3 Specimen testing setup

2.3 Testing Methodology

The slump test was carried out in accordance with ASTM C143 (ASTM, 2015) specifications. The vertical distance between the top of the inverted mold and the center of the top surface of the concrete mixture was used to calculate the slump value. At 28 days, the compressive strength and splitting tensile strength of three specimens of hardened concrete were evaluated. Three specimens' worth of results were averaged out to obtain the results. In accordance with BS EN (EN, 2009), compression strength tests were performed on cube specimens (150 mm) using hydraulic equipment with a 500 kN capacity. Up until the specimens failed, an axial force was applied continuously at a rate of 4.5 kN/s. Following ASTM C496 (ASTM, 2011), splitting tensile strength tests were carried out on the cylinder specimens (100 × 200 mm). The loading rate used was 0.9 MPa/min.

Five RC beams made up the test specimens, which were put to the test under four-point flexural loading. Details of the RC beam specimens are shown in Table 5. The RC beams had a depth of 200 mm, a width of 100 mm, and a length of 1500 mm. The beams had a 1400 mm effective span. The bottom of the RC beam had longitudinal 2Ø10 reinforcing rebars for flexural tensile, and the top reinforcing rebars, which served as compression reinforcement and were primarily used to support shear stirrups, had longitudinal 2Ø8 reinforcing rebars. The RC beams were equipped with 100 mm center-to-center, two-legged, 8 mm vertical shear stirrups. The dimensions and reinforcing details are shown in Fig. 3. The specimens were constructed and cast, as well as quasi-statically tested using testing frames with flexural capacities that could support 500 kN on the testing floor in the Structures Lab in the Department of Civil Engineering at Kafrelsheikh University, Kafrelsheikh, Egypt. In order to have more time to record the test results and capture the crack pattern, the loading rate was kept comparatively low. Fig. 3 displays a picture of the specimen along with the testing setup.

2.4 Strengthening Schemes

Fig. 4 displays the strengthened beams in more detail. The first beam (i.e., SDC-E) was strengthened by a wooden plate, which was fixed to the beams by an adhesive layer, as shown in Fig. 4b. The dimensions of the wooden plate are a depth of 20 mm, a width of 100 mm, and a length of 1100 mm. The type of adhesive layer was Sikadur 330. Table 6 shows the properties and preparation of the adhesive material used in this study. The second and third beams (i.e., SDC-2A and SDC-11A) were

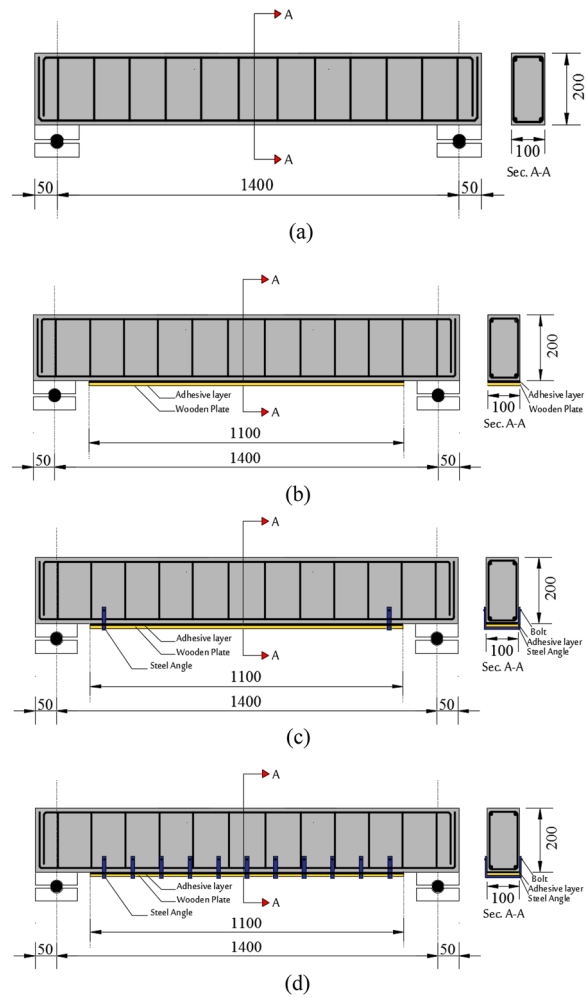

Fig. 4 The details of strengthening schemes for RC beams: **a** NC-1 and SDC-1; **b** SDC-E; **c** SDC-2A; and **d** SDC-11A

Table 5 Specimens tested for RC beams

Specimen ID	Concrete mix	Strengthening	Strengthening type
NC-1	NC	None	None
SDC-1	SDC	None	None
SDC-E	SDC	Yes	Wooden plate fixed by epoxy resin (see Fig. 4b)
SDC-2A	SDC	Yes	Wooden plate fixed by epoxy resin and two steel angles (see Fig. 4c)
SDC-11A	SDC	Yes	Wooden plate fixed by epoxy resin and eleven steel angles (see Fig. 4d)

Table 6 Properties and preparation of the adhesive materials used in this study

Material	Manufacturer	Color	Preparation method
Sikadur 330	Sika	Grey	Mixing a two-component (an epoxy-based resin) and putting it on the RC beam and the wood strengthening plate surfaces

strengthened by a wooden plate, which was fixed to the beams by an adhesive layer, then fixed to the beams by two and eleven steel angles (80 × 80 × 8 mm) in each face of the beam, respectively, as shown in Fig. 4c, d. The yield stress of the steel angles was 240 MPa.

3 Results and Discussion

3.1 Workability

The results of the slump tests for each concrete mixture are shown in Table 7. According to the slump results, using SD as a partial sand replacement significantly reduced the workability of fresh concrete. The SDC mixture produced a slump value of 10 mm, which was lower than the control mixture (i.e., NC) by 20 mm. This can be attributed to several causes, including: (i) the inclusion of SD might create a network structure in the concrete mixture; (ii) the increased air content, which causes a high porosity; (iii) the increased density of SDC mixtures as a result of the low specific gravity of SD (2.12) compared with fine aggregates (2.50); all those reasons can lead to a major loss in workability (Ahmed et al., 2018; Batool et al., 2021; Oyedepo et al., 2014).

3.2 Compressive Strength

Table 7 depicts the compressive strength of normal and SDC mixtures containing SD. According to the results, using SD as a partial sand replacement significantly reduced the compressive strength of the SDC mixture. The SDC mixture produced a compressive strength of 19 MPa, which was lower than the control mixture (i.e., NC) by 62%. This can be attributed to the SD's high water absorption capacity and porous nature. Thus, leaving an inadequate quantity of water negatively affects the process of hydration (Batool et al., 2021; Opiso et al., 2019). According to Vaidkelionis and Vaickelionene (2006), the hydration procedures are slowed down as a result of the inclusion of wood extractives, which contributes to the decreased compressive strength. This is mostly because SD and fine aggregate have different chemical compositions, which causes a weaker connection to form in the concrete matrix. The compressive strength is highly reduced by the weak interfacial transition zones between cement paste and aggregates (Siddique et al., 2020). In addition, the porous nature of SD and the reduced density of concrete may both be contributing factors to the reduction in compressive strength (Batool et al., 2021).

3.3 Splitting Tensile Strength

The results of the splitting tensile tests for each concrete mixture are shown in Table 7. The inclusion of SD significantly reduced the splitting tensile strength. The NC and SDC mixtures produced a splitting tensile strength of 4 and 2 MPa, respectively, where SDC exhibited a lower splitting tensile strength by 62% compared with the NC mixture. This result is consistent with the literature study's findings (Ahmed et al., 2018; Batool et al., 2021; Foti & Cavallo, 2018). Ahmed et al. (2018) reported that the inclusion of SD weakens the interfacial transition zones and reduces the tensile strength as a result of heterogeneous discontinuities in the SDC matrix. Additionally, Foti and Cavallo (2018) mentioned that this reduction can be attributed to the weak connection between cement mortar and SD particles.

3.4 Failure Modes and Crack Pattern

Fig. 5 shows the ultimate failure modes and crack patterns for all RC beams. In addition, Table 8 summarizes the description of the crack pattern and the beams' failure modes. The main flexural cracks in the control specimens (i.e., NC-1) rapidly expanded from the tension side (i.e., bottom surfaces) in the direction of the applied load points at the top surfaces (i.e., compression

Table 7 NC and SDC mixtures' properties

Mechanical properties	NC			Average	STDV	SDC			Average	STDV
	Sample (1)	Sample (2)	Sample (3)			Sample (1)	Sample (2)	Sample (3)		
Slump value (mm)	21	19	20	20	1	10	11	10	10	0.58
Compressive stress (MPa)	29	32	31	31	1.5	17	20	20	19	1.7
Splitting tensile stress (MPa)	5	4	4	4	0.6	2	2	3	2	0.6

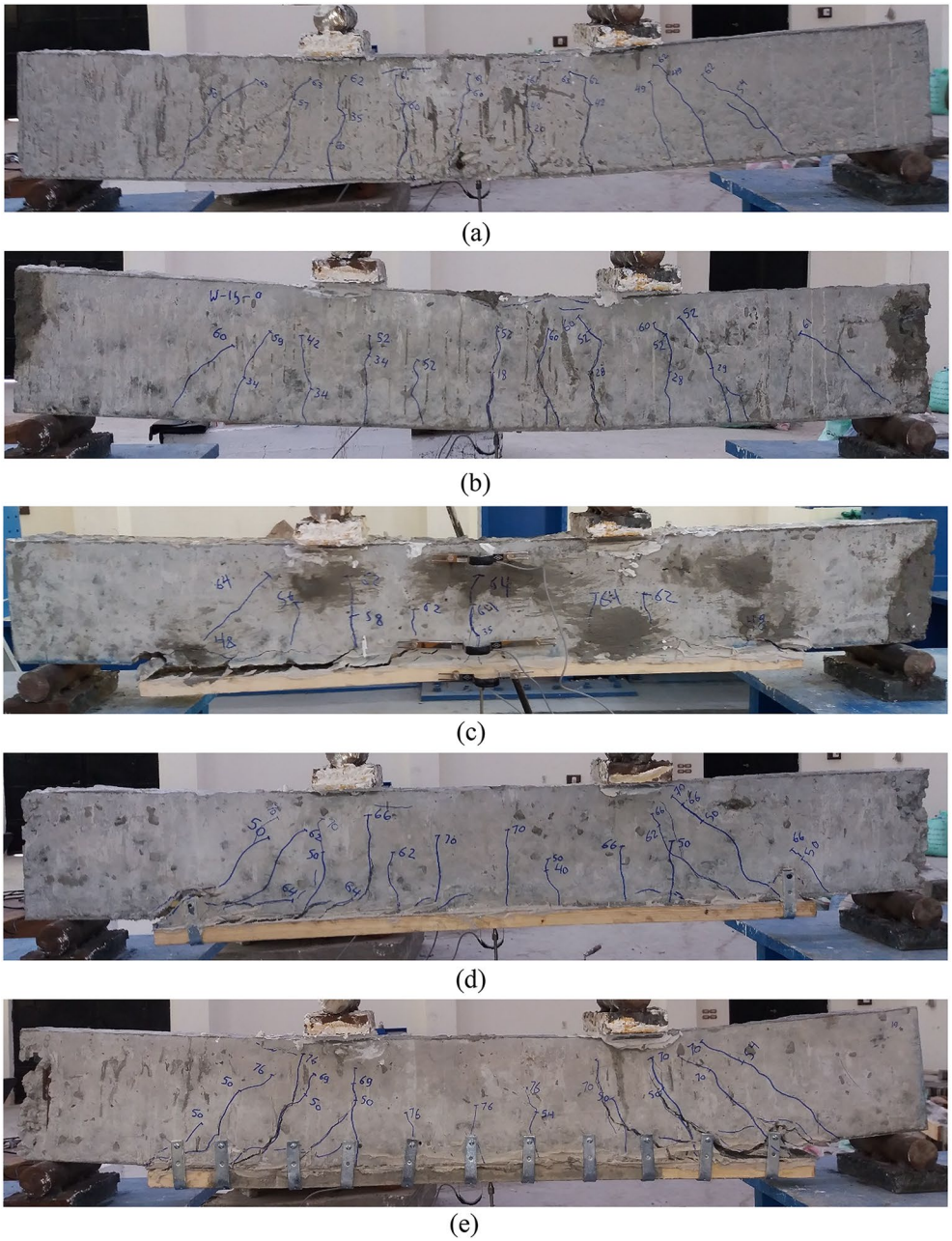

Fig. 5 Crack patterns and failure modes of RC beams: **a** NC-1; **b** SDC-1; **c** SDC-E; **d** SDC-2A; and **e** SDC-11A

Table 8 Description of the crack pattern and beams' failure modes

Specimen ID	Shear cracks	Flexural cracks	Concrete crushing
NC-1	Fewer, narrow, short	Numerous flexural crack	None
SDC-1	Fewer, narrow, short	Major and narrow flexural cracks	Crushing at the compression zone between load points
SDC-E	Fewer, narrow, short	Fewer, narrow, short	Close to the left support, separation occurred with a layer of concrete on the wooden plate
SDC-2A SDC-11A	Significant diagonal cracks close to the left/right support	Fewer, narrow, short	Separation of the concrete surrounding the steel angle and debonding of the wooden plate edge on the left/right support

side) in the middle of the beam, as shown in Fig. 5a. As the applied load increased, numerous cracks were generated and concentrated in the same areas. The formation of those cracks was caused by the positive flexure bending moment at the indicated area. After that, new cracks developed and propagated through the entire cross-section of the beam, resulting in a sudden drop in the flexural resistance. The beam failed because it was unable to maintain its capability for load resistance. Additionally, there was no evidence of concrete crushing in the compressive zone as a result of the higher compressive strength. Demonstrating the flexural failure mode of a typical RC beam, the first flexural crack appeared at the applied load of 20 kN, while the first shear crack appeared at the applied load of 54 kN. In general, the failure mode and crack pattern of the NC-1 and SDC-1 specimens were nearly similar, excluding the appearance of concrete crushing at the compression zone for the SDC-1 beam. When testing started, a tension zone in the beam's mid-span generated a number of flexural cracks. The strength of the NC-1 and SDC-1 beams has been impacted by the many cracks that developed at the beam's mid-span, increasing the curvature. The beams failed due to their inability to maintain load resistance capacity. The failure mode for the SDC-1 beam was a flexural failure, as shown in Fig. 5b. The first flexural crack appeared at the applied load of 18 kN, while the first shear crack appeared at the applied load of 61 kN. The reported flexural failure was characterized by a single flexural crack in the middle-third of the SDC-1 beam, extending upward to the top fiber of the concrete between the load points. Regarding the SDC-E beam, the first vertical flexure cracks began to appear in the beam's mid-span at 35 kN, followed by separation in the wooden plate at the ends near the left supports at a load of 48 kN. The first shear crack appeared at the applied load of 64 kN. With the increase in loading, the separation began to gradually increase inward towards the loading points, with the appearance of new vertical cracks until failure. Additional cracks in the compression zone started at a load of 58 kN. A flexure-shear crack at the shear span limits the capacity of beams to support greater loads. The failure mode for the SDC-E beam was shear failure. The first strengthening scheme did not improve the SDC-E beam's flexural strength, which prevented further deformation and energy absorption by the beams, causing shear failure rather than flexural failure. Additionally, there was no evidence of concrete crushing in the compressive zone. As shown in Fig. 5c, separation of the wooden plate occurred along with an attached thin layer of concrete on it. It can be noticed that there are no cracks in the wooden plate. For the SDC-2A beam, the first vertical flexure cracks began to appear in the beam's mid-span at 40 kN, then an inclined shear crack (i.e., roughly 45 degrees from a horizontal direction) occurred at the end of the wooden plate and moved towards the loading points at 50 kN. After that, two parallel cracks appeared at 66 kN, a separation of the fixing angle occurred around the bolts, and the concrete surrounding the bolts collapsed with the presence of cracks in the compression zone, as shown in Fig. 5d. Flexural cracks' growth is very slow with the increased loading; only the already-existing shear cracks expanded. After the complete collapse of the anchorage area, the concrete cover separation began to appear at 64 kN. As the loading reached 70 kN, debonding occurred at the edge of the wooden plate on the left support. The failure mode for the SDC-2A beam was shear failure. The second strengthening scheme improved the SDC-2A beam's flexural strength and changed the failure mode so it was controlled by shear failure rather than flexural failure. Major flexural cracks, however, were not present in this beam. Additionally, there was no evidence of concrete crushing in the compressive zone. This specimen displayed increased flexural strength and stiffness together with ductile post-peak behavior, which increases the ability of the beam to undergo significant deformations before total failure. Consequently, the occupants receive early warning before failure. In general, the failure mode and crack pattern of the SDC-2A and SDC-11A specimens were nearly similar. The appearance of the first flexural and shear cracks occurred at the same time at 50 kN and a deformation of 19 mm. After that, a separation of the fixing angle occurred around the bolts, and the concrete surrounding the bolts collapsed near the right support, which dominated the beam behavior, as shown in Fig. 5e. With increasing loading, the shear crack width increased in the critical shear zone, and the SDC-11A beam failed in shear mode. In contrast to shear cracks, however, flexural cracks did not significantly expand. In contrast to SDC-2A, the third strengthening scheme did not improve the SDC-11A beam's flexural strength, which prevented further deformation and energy absorption by the beams, causing shear failure rather than flexural failure.

3.5 Load–Displacement/Strains Characteristics

Fig. 6 provides the load–deflection (mid-span deflection) curves for all of the beams. The load–deflection behavior initially resembles that of an uncracked beam. The curve development in this segment is regarded as steeply linear. After the first section, as can be seen, these curves began to diverge from one another. Concrete cracking caused the slope of the load–deflection behavior to decrease, displaying nonlinear behavior. The deflection of all specimens was continued with a slight increase in the applied load. Then, until the

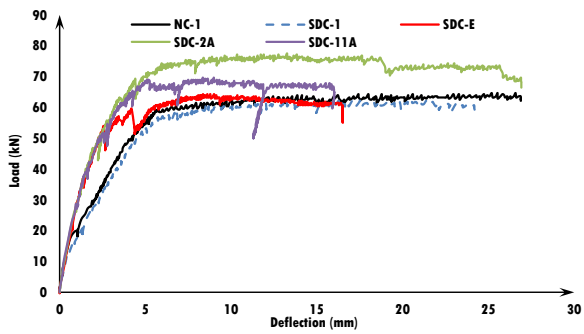

Fig. 6 Load–deflection curves of all RC beams

failure of the beams, the same status continued. Specimen NC-1 had a maximum flexure strength of 64.62 kN at a displacement of 25.53 mm. Due to material nonlinearity, the specimen displayed almost stability resistance (slightly decreased from 64.62 to 62.12 kN) to the applied load as vertical displacement increased after the maximum strength was reached. An abrupt decrease in applied load may have been caused by the rupture of reinforcing steel bars when the applied load attained 62.118 kN at a vertical displacement of 26.89 mm. From the initial loading until the maximum flexure strength, the reaction of SDC-1 was identical to that of NC-1, after which the flexure resistance of SDC-1 was less in comparison to NC-1. As the vertical displacement increased after the maximum flexural resistance was attained, the flexure strength was almost stable (slightly decreased from 62.12 to 59.26 kN) until the abrupt decrease in the applied load. The SDC-1 beam failed at 59.262 kN flexure strength and a displacement of 24.19 mm. As shown in Fig. 6, the NC-1 and SDC-1 beams demonstrated ductile failure, meaning that the entire beam's deflection continued as the applied load increased. Even with the inclusion of SD, the ultimate load in the SDC-1 beam was lower than in the NC-1 beam (i.e., without SD), with a slight variation of approximately 4%. Regarding specimen SDC-E, the maximum flexure strength was 64.26 kN at a displacement of 8.36 mm. As the vertical displacement increased after the maximum flexural capacity was achieved, the flexural resistance progressively began to decline until the first drop (i.e., from 59.62 to 51.41 kN) at 4.39 mm of displacement. This can be attributed to the separation that occurred with the layer of concrete on the wooden plate, as shown in Fig. 5c. The SDC-E beam was able to sustain a higher flexural resistance when the load–deflection curve began to increase once more. The second sudden drop in flexural capacity may have been caused by the rupture of reinforcing steel bars when the applied load reached 54.98 kN at a vertical displacement of 16.51 mm. Specimen SDC-2A had a maximum flexure strength of 77.47 kN at a displacement of 13.26 mm. Up to a displacement of 173.5 mm, the flexural strength nearly remained unchanged, then the first sudden drop occurred at 19.26 mm of displacement (i.e., from 76.39 to 70.33 kN). This can be attributed to the separation of the concrete surrounding the steel angle and the debonding of the wooden plate edge on the right support, as shown in Fig. 5d. After this load level, the load–deflection curve began ascending again, and the SDC-2A was able to withstand greater flexural resistance as the vertical displacement increased. The second sudden drop in flexural capacity may have been caused by the rupture of reinforcing steel bars when the applied load reached 66.40 kN at a vertical displacement of 26.92 mm. For specimen SDC-11A, the maximum flexure strength was 69.62 kN at a displacement of 8.35 mm. As the vertical displacement increased after the maximum flexural capacity was achieved, the flexural resistance progressively began to decline until the first sudden drop (i.e., from 68.90 to 60.69 kN) at 6.87 mm of displacement. The second sudden drop from 68.54 to 49.98 kN was recorded at 11.29 mm of displacement. This can be attributed to the separation of the concrete surrounding the steel angle and the debonding of the wooden plate edge on the right support, as shown in Fig. 5e. The SDC-11A beam was able to sustain a higher flexural resistance when the load–displacement curve began to increase once more. The third sudden drop in flexural capacity may have been caused by the rupture of reinforcing steel bars when the applied load reached 59.98 kN at a vertical displacement of 15.88 mm. The large extent of the crack led to a significant drop in the amount of resistance capacity for SDC-E and SDC-11A beams in their nonlinear behavior (i.e., second-segment slopes). The SDC-E and SDC-11A beams' deflection abruptly stopped; these findings demonstrate a brittle failure mode. It can be observed that, despite the inclusion of SD, the strengthening schemes using the two steel angles (i.e., SDC-2A) significantly influenced the growth of the beams' ultimate load compared with all specimens. The peak load capacities were 64.62, 62.12, 64.26, 77.47, and 69.62 kN for these mixtures: NC-1, SDC-1, SDC-E, SDC-2A, and SDC-11A, respectively. Additionally, the SDC-2A exhibited the highest peak load when compared to all other mixes, with increased ratios of 16.58, 19.81, 17.05, and 10.13% compared with NC-1, SDC-1, SDC-E, and SDC-11A, respectively. Fig. 7 illustrates another indicator of the flexural resistance capacity, which was the specimen's energy absorption (the area enclosed under the load–deflection curves). The inclusion of SD in the beam has reduced

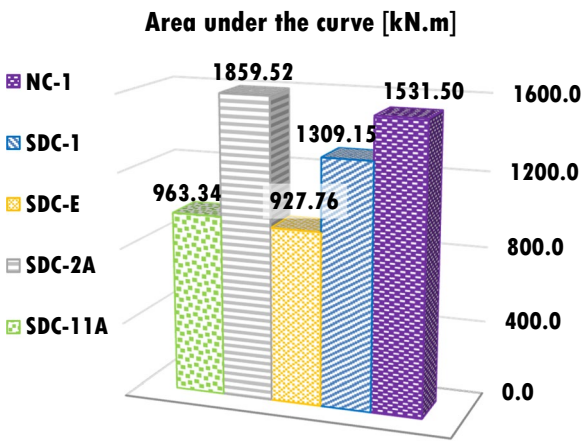

Fig. 7 The specimen's energy absorption of all RC beams

the SDC-1 beam's energy absorption by 14.5% compared with NC-1. The first strengthening scheme (i.e., SDC-E) exhibited lower energy absorption; the reduction ratio reached 39.4, 29.1, 50.1, and 0.9% compared with NC-1, SDC-1, SDC-2A, and SDC-11A, respectively. Moreover, the second strengthening scheme (i.e., SDC-2A) exhibited the highest energy absorption; the increased ratio reached 17.64, 29.6, 50.1, and 49.6% compared with NC-1, SDC-1, SDC-E, and SDC-11A, respectively. The use of eleven steel angles in the SDC-11A led to a negative effect by recording a reduction in the beam's energy absorption by 49.6% compared with the use of two steel angles in the second strengthening scheme (i.e., SDC-2A). Therefore, the SDC-2A demonstrates superior deformation properties compared with all other beams. Fig. 8 shows the load-strain curves based on the readings from the PI displacement transducers used to measure strains in concrete surfaces and wooden plates. The strain curves exhibit a few interruptions, which may be the result of the cracks' sudden formation near PI gauges. As expected, the readings of the PI gauges on the upper concrete surfaces showed compressive and tensile strains in the measurements on the lower concrete surfaces as well as on wooden plates. The compression strain values of the concrete surface were higher in the SDC-1 beam than in the NC-1 beam, as shown in Fig. 8a, b. This demonstrated unequivocally that the SDC-1 beam showed more cracks (concrete crushing) at the compression zone than those of the NC-1 beam, as also shown in Fig. 5b. As shown in Fig. 8a, c, the compression strain values of the concrete surface in the SDC-E beam were nearly identical to those in the NC-1 beam. Unfortunately, the readings of the PI gauges in the tension zone did not continue to measure the strains in the SDC-E, SDC-2A,

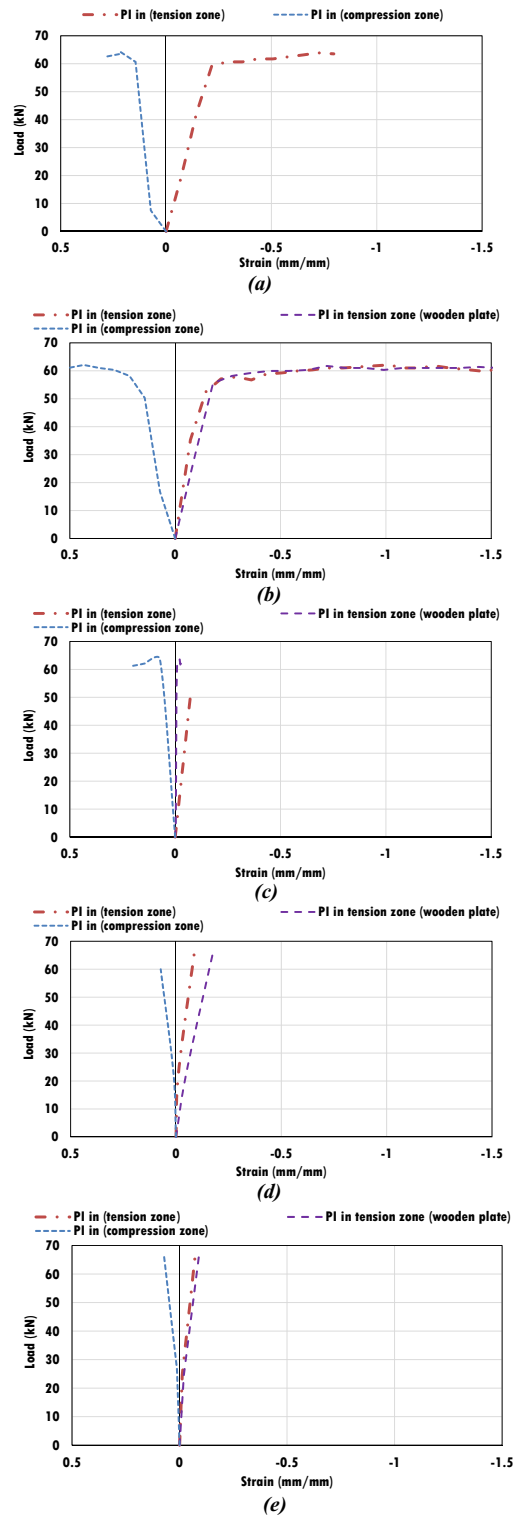

Fig. 8 Load-strain curves of RC beams: **a** NC-1; **b** SDC-1; **c** SDC-E; **d** SDC-2A; and **e** SDC-11A

and SDC-11A beams (see Fig. 8c, d, e), as the PI gauges were separated from the concrete surfaces and wooden plates. However, the PI gauges in the compression zones in the SDC-2A and SDC-11A beams recorded small strain values compared with the NC-1, SDC-1, and SDC-E beams, which indicated a brittle failure in the SDC-2A and SDC-11A beams.

3.6 Ultimate Load Capacity

The deformability factors (DF), normalized strength factors (SF), and overall structural performance factors (PF), which illustrate a structural element's ability to withstand plastic deformation after reaching peak load capacities, were used to evaluate the effectiveness of the inclusion of SD and the strengthening schemes (Abdal et al., 2023; Abdullah et al., 2022; Al-Rousan, 2017; Fayed & Mansour, 2020; Mansour & Fayed, 2021; Mansour et al., 2022). Table 9 shows the tested specimens' performance factors. Table 9 demonstrates that the inclusion of SD in the beam has reduced the SDC-1 beam's deformation and strength by 10% and 4%, respectively, as well as the overall structural performance factors by 14%. It can be observed that, despite the application of strengthening schemes using only wooden plates (i.e., SDC-E), the SDC-E beam's deformation and strength have been reduced by 39% and 1%, respectively, as well as the overall structural performance factors by 40%. Despite the inclusion of SD, the application of strengthening schemes by a wooden plate and two steel angles (i.e., SDC-2A) can totally restore the DF, SF, and PF with ratios up to 100, 120, and 120%, respectively. Regarding the application of strengthening schemes by a wooden plate and eleven steel angles (i.e., SDC-11A), this has reduced the SDC-11A beam's deformation and the overall structural performance factor by 40% and 35%, respectively. However, the beam's strength factor increased by 8% compared with NC-1 (i.e., the control specimen). Additionally, if we take into account the combined strength (i.e., SF) and the deformation performance (i.e., PF), the inclusion of SD and the strengthening schemes used in this study give a highly promising result.

Table 9 Tested specimens' performance variables

Specimen ID	NC-1	SDC-1	SDC-E	SDC-2A	SDC-11A
Max. deflection Δ_u (mm)	26.89	24.19	16.51	26.92	16.01
DF = Δ_u/Δ_u (NC-1 control)	–	0.90	0.61	1.00	0.60
Ultimate load P_u (kN)	64.62	62.12	64.26	77.47	69.62
$SF = P_u/P_u$ (NC-1 control)	–	0.96	0.99	1.20	1.08
PF = DF*SF	–	0.86	0.60	1.20	0.65

3.7 Effectiveness of Strengthening Scheme

The peak load capacity of the tested specimens is represented graphically in Fig. 9a as a bar chart. Fig. 9b provides the beam's mid-span deflection at maximum load. Among all the beams, the SDC-2A beam shows the highest load-carrying capacity (due to enhanced flexural strength) compared with all other beams. Additionally, the SDC-2A beam outperformed all strengthening beams in terms of post-peak performance in strength deterioration (Fig. 6). The early stiffness properties of all strengthening beams (i.e., SDC-E, SDC-2A, and SDC-11A) were improved compared with unstrengthening beams (i.e., NC-1 and SDC-1), as shown in Fig. 6. The SDC-E and SDC-11A beams' deflection abruptly stopped; these findings demonstrate a brittle failure mode. Moreover, the peak loads of SDC-E and SDC-11A beams were reached at 8.36 and 8.35 mm, respectively, which prevented further deformation and energy absorption by the beams,

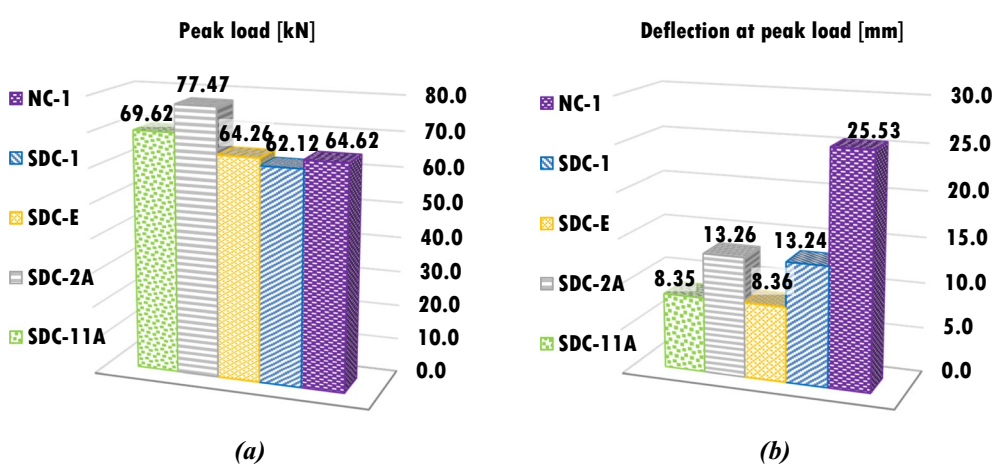

Fig. 9 Peak load of tested beams and the corresponding deflection: **a** peak load and **b** mid-span deflection at peak load

as shown in Fig. 9b. It can be observed that the implementation of strengthening schemes by increasing the steel angles (i.e., SDC-11A) had the opposite effect on post-peak performance in terms of strength deterioration compared with SDC-2A (see Fig. 6). The peak load capacities of NC-1, SDC-1, and SDC-E were nearly the same. In addition to preventing post-peak strength loss, the application of strengthening schemes using a wooden plate and two steel angles enhanced the flexural strength and ductility capabilities of beams. The increased ductility of the beams may be advantageous for seismic resistance. The SDC-11A strengthening plan increased peak load. However, compared to the control specimen (i.e., NC-1), the beam's deflection capacity was not improved (see Fig. 6). Moreover, the strengthening scheme used in SDC-E showed a slight reduction in the peak load, and the beam's deflection capacity was not improved compared to the control specimen.

4 Comparison of Current Research Findings with Previous Studies

Table 10 shows the concrete mixture design of normal concrete as well as sawdust concrete for current research and compares their results in terms of compressive and tensile strengths with the previous results available in the literature. In general, all investigations concurred with the current research findings that the compressive and tensile strengths decreased as the sawdust ratio in the concrete mixture increased. Therefore, designers must take caution and carefully select the sawdust ratio within the concrete mixture when employing such design mixtures in real engineering applications to prevent the employed concrete from losing the majority of its resistance to compression or tension. Siddique et al. (2020) explained in their study that the compressive resistance of concrete decreased from 26 to 10 MPa when 20% of the volume of sand was replaced with sawdust instead of 10%, and the tensile resistance decreased from 2.8 to 1.3 MPa at the same replacement ratios. Moreover, the highest compressive-to-tensile ratio was recorded at a 10% replacement rate. The compressive and tensile strengths of sawdust concrete entirely destroyed when a high sawdust ratio was used, as Batool et al. (2021) concluded. When compared to the results of the reference sample, which contains no sawdust, the compressive resistance reduced by 93% and the tensile resistance decreased by 88% at a 60% replacement ratio.

Specifically, the findings demonstrate that the compressive and tensile strengths of sawdust concrete depend not only on the proportion of sawdust to sand but also on the cement content and aggregate content, whether coarse or fine, within the concrete mixture. Table 10 shows how a larger cement and aggregate content reduces the loss in compressive and tensile strengths at the same replacement ratio. At a 15% replacement ratio, the reduction in compressive strength was 50, 12, 9, and 39% at cement content of 394, 416, 400, and 400 kg/m^3 and coarse aggregate content of 970, 1041, 1141, and 1300 kg/m^3, respectively. The current analysis comes to the conclusion that the compressive and tensile strengths of sawdust concrete are greatly influenced by the amount of cement and aggregate in the concrete mixture. Therefore, additional experimental studies are required to comprehend the relationship between compressive and tensile resistance when the cement and aggregate content of the concrete mixture changes while maintaining a constant sawdust ratio.

5 Conclusion

The following are the main conclusions made from the experimental findings of this study:

1. Sawdust concrete can be employed in construction projects to reduce environmental degradation as a result of excessive use of natural aggregates and improper disposal of these wastes.
2. The concrete's workability, compressive, and splitting tensile strengths were reduced with the addition of SD as a substitute for fine aggregates. The reduction ratios reached 10%, 62%, and 30% for workability, compressive, and splitting tensile strengths, respectively, compared with the control mixture.
3. The failure mode and crack pattern of the NC-1 and SDC-1 specimens were nearly similar. The failure mode for the NC-1 and SDC-1 beams was a flexural failure. On the contrary, the failure mode for all the strengthened beam specimens (i.e., SDC-E, SDC-2A, and SDC-11A) was shear failure.
4. According to the load–deflection curves, the NC-1, SDC-1, and SDC-2A beams demonstrated ductile failure, while the SDC-E and SDC-11A beams showed a brittle failure mode.
5. The inclusion of SD in the beam has reduced the SDC-1 beam's DF and SF by 10% and 4%, respectively, as well as PF by 14%.
6. The application of strengthening schemes with a wooden plate and two steel angles (i.e., SDC-2A) can totally restore the DF, SF, and PF with ratios up to 100%, 120%, and 120%, respectively. While the remaining strengthening schemes have reduced the overall structural performance factor.
7. The SDC-2A strengthening plan outperformed all strengthening beams in terms of load-carrying capacity and post-peak performance in strength deterioration.

Table 10 Mix design, compressive, and tensile strength of SDC with respect to previously published results

References	ID	Cement (kg/m^3)	Aggregate		SD		Water	Compressive strength, C (MPa)	Tensile strength, T (MPa)	C/T
			Coarse (kg/m^3)	Fine (kg/m^3)	Weight (kg/m^3)	Ratio by volume				
Siddique et al. (2020)	CA	394	970	818	0	0	197	28	2.9	9.7
	AW5			777	41	5		26	2.8	9.3
	AW10			736	82	10		20	2.0	10
	AW15			695	123	15		14	1.7	8.2
	AW20			654	164	20		10	1.3	7.7
Ahmed et al. (2018)	NWC	416	1041	625	0	0	208	38.8	Not provided	Not provided
	05SD			594	5.25	5		37.8		
	10SD			562	10.50	10		36		
	15SD			531	15.75	15		34.2		
Dias et al. (2022)	REF	400	1141	690	0	0	162	64	Not provided	Not provided
	SD5			598	60	5		63		
	SD10			507	121	10		59		
	SD15			415	181	15		58		
Batool et al. (2021)	SD0	420	1260	840	0	0	189	27	2.5	10.8
	SD10			756	84	10		23	2.4	9.6
	SD20			672	168	20		18	1.7	10.6
	SD30			588	252	30		7	0.8	8.8
	SD40			504	336	40		5.5	0.5	11
	SD50			420	420	50		3.5	0.4	8.8
	SD60			336	504	60		1.9	0.3	6.3
Current study	NC	400	1300	650	0	0	240	31	4	7.8
	SDC	400	1300	552.5	10.9	15	240	19	2	9.5

8. The study's findings offered useful information for developing eco-friendly sawdust concrete beams with efficient strengthening techniques for potential future uses.

6 Future Work and Recommendations

Chemical compositions of hydration products and thermo mechanical properties in SDC mixtures, as well as EDS analysis of cracked SDC mixtures, should all be investigated in further research.

Acknowledgements
The authors are thankful to the Deanship of Scientific Research at Najran University for funding this work under the General Research Funding program Grant Code (NU/DRP/SERC/12/21).

Author Contributions
AMM: Conceptualization, Methodology, Idea of the research, Writing, Writing-review, Supervision and editing. WM: Conceptualization, Methodology, Idea of the research, Writing, Writing-review, Supervision and editing. SF: Methodology, Idea of the research, Writing, Writing-review, Supervision and editing. BT: Conceptualization, Methodology, Idea of the research, Writing, Writing-review and editing. AMY: Conceptualization, Methodology, Writing, Writing-review, Supervision and editing. MH: Writing and Writing-review. All authors read and approved the final manuscript.

Availability of Data and Materials
Some of all the data, models, or code that support the findings of this study are available from the corresponding author upon reasonable request.

Declarations

Ethics Approval and Consent to Participate
None.

Consent for Publication
None.

Competing Interests
No potential competing interests was reported by the authors.

Received: 28 February 2023 Accepted: 21 May 2023
Published: 12 September 2023

References

Abadel, A., Abbas, H., Almusallam, T., Alshaikh, I. M., Khawaji, M., Alghamdi, H., & Salah, A. A. (2022). Experimental study of shear behavior of CFRP strengthened ultra-high-performance fiber-reinforced concrete deep beams. *Case Studies in Construction Materials, 16*, e01103.
Abdal, S., Mansour, W., Agwa, I., Nasr, M., Abadel, A., Onuralp Özkılıç, Y., & Akeed, M. H. (2023). Application of ultra-high-performance concrete in bridge engineering: Current status, limitations, challenges, and future prospects. *Buildings, 13*(1), 185.
Abdullah, G. M., Alshaikh, I. M., Zeyad, A. M., Magbool, H. M., & Bakar, B. A. (2022). The effect of openings on the performance of self-compacting concrete with volcanic pumice powder and different steel fibers. *Case Studies in Construction Materials, 17*, e01148.
ACI-211. (2002). *Standard practice for selecting proportions for normal, heavy-weight and mass concrete*. Farmington Hills, MI, USA: American Concrete Institute.
ACI-308R-01-R08. (2008). *Guide to curing concrete*. ACI Committee 308
Ahmed, A., & Kamau, J. (2017). A review of the use of corncob ash as a supplementary cementitious material. *European Journal of Engineering and Technology Research, 2*(8), 1–6.
Ahmed, W., Khushnood, R. A., Memon, S. A., Ahmad, S., Baloch, W. L., & Usman, M. (2018). Effective use of sawdust for the production of eco-friendly and thermal-energy efficient normal weight and lightweight concretes with tailored fracture properties. *Journal of Cleaner Production, 184*, 1016–1027.
Aksoylu, C. (2022). Shear strengthening of reinforced concrete beams with minimum CFRP and GFRP strips using different wrapping technics without anchoring application. *Steel and Composite Structures*. https://doi.org/10.12989/scs.2022.44.6.831
Al-Rousan, R. (2017). Influence of polypropylene fibers on the flexural behavior of reinforced concrete slabs with different opening shapes and sizes. *Structural Concrete, 18*(6), 986–999.
Alshaikh, I. M., Abadel, A. A., Sennah, K., Nehdi, M. L., Tuladhar, R., & Alamri, M. (2022). Progressive collapse resistance of RC beam-slab substructures made with rubberized concrete. *Buildings, 12*(10), 1724.
Altun, F. (2004). An experimental study of the jacketed reinforced-concrete beams under bending. *Construction and Building Materials, 18*(8), 611–618.
Alwesabi, E. A., Bakar, B. A., Alshaikh, I. M., & Akil, H. M. (2020). Experimental investigation on mechanical properties of plain and rubberised concretes with steel–polypropylene hybrid fibre. *Construction and Building Materials, 233*, 117194.
Amin, M., Zeyad, A. M., Tayeh, B. A., & Agwa, I. S. (2022). Effect of ferrosilicon and silica fume on mechanical, durability, and microstructure characteristics of ultra high-performance concrete. *Construction and Building Materials, 320*, 126233.
ASTM-C143. (2015). *Standard specification for standard test method for slump of hydraulic-cement concrete*. West Conshohocken, PA, United States: American Society for Testing and Materials.
ASTM-C150. (2007). *Standard test method for Portland cement*. West Conshohocken, PA, United States: American Society for Testing and Materials.
ASTM-C33. (2016). *Standard specification for concrete aggregates*. West Conshohocken, PA, United States: American Society for Testing and Materials.
ASTM-C33/C33M. (2018). *Standard specification for concrete aggregates*.
ASTM-C496. (2011). *Standard test method for splitting tensile strength of cylindrical concrete specimens*.
ASTM-E8. (2009). *Standard test methods for tension testing of metallic materials*.
Batool, F., Islam, K., Cakiroglu, C., & Shahriar, A. (2021). Effectiveness of wood waste sawdust to produce medium-to low-strength concrete materials. *Journal of Building Engineering, 44*, 103237.
Butt, W. A., Gupta, K., & Jha, J. N. (2016). Strength behavior of clayey soil stabilized with saw dust ash. *International Journal of Geo-Engineering, 7*, 1–9.
Cheah, C. B., & Ramli, M. (2013). The engineering properties of high performance concrete with HCWA–DSF supplementary binder. *Construction and Building Materials, 40*, 93–103.
Dias, S., Tadeu, A., Almeida, J., Humbert, P., António, J., de Brito, J., & Pinhão, P. (2022). Physical, mechanical, and durability properties of concrete containing wood chips and sawdust: An experimental approach. *Buildings, 12*(8), 1277.
Elsayed, M., Tayeh, B. A., Aisheh, Y. I. A., Abd El-Nasser, N., & Abou, E. M. (2022). Shear strength of eco-friendly self-compacting concrete beams containing ground granulated blast furnace slag and fly ash as cement replacement. *Case Studies in Construction Materials, 17*, e01354.
EN, B.S., 12390-3 (2009). *Testing hardened concrete—Part 3: Compressive strength of test specimens*. British Standards Institution.
Faried, A. S., Mostafa, S. A., Tayeh, B. A., & Tawfik, T. A. (2021). The effect of using nano rice husk ash of different burning degrees on ultra-high-performance concrete properties. *Construction and Building Materials, 290*, 123279.
Fayed, S., & Mansour, W. (2020). Evaluate the effect of steel, polypropylene and recycled plastic fibers on concrete properties. *Advances in Concrete Construction, 10*(4), 319–332.
Foti, D., & Cavallo, D. (2018). Mechanical behavior of concretes made with non-conventional organic origin calcareous aggregates. *Construction and Building Materials, 179*, 100–106.
Habert, G., Bouzidi, Y., Chen, C., & Jullien, A. (2010). Development of a depletion indicator for natural resources used in concrete. *Resources, Conservation and Recycling, 54*(6), 364–376.

Hakeem, I. Y., Agwa, I. S., Tayeh, B. A., & Abd-Elrahman, M. H. (2022). Effect of using a combination of rice husk and olive waste ashes on high-strength concrete properties. *Case Studies in Construction Materials, 17*, e01486.
Hamada, H., Tayeh, B., Yahaya, F., Muthusamy, K., & Al-Attar, A. (2020). Effects of nano-palm oil fuel ash and nano-eggshell powder on concrete. *Construction and Building Materials, 261*, 119790.
Jeevan, N., Gowda, B. K., Archana, D. P., Razak, A., Abbas, M., & Saleel, C. A. (2023). Experimental study on flexural strengthening of rc beams with nsm technique by different orientation of cfrp laminate. *Ain Shams Engineering Journal, 14*(1), 101823.
Khan, E. U., Khushnood, R. A., & Baloch, W. L. (2020). Spalling sensitivity and mechanical response of an ecofriendly sawdust high strength concrete at elevated temperatures. *Construction and Building Materials, 258*, 119656.
Mageswari, M., & Vidivelli, B. (2009). The use of sawdust ash as fine aggregate replacement in concrete. *Journal of Environmental Research and Development, 3*(3), 720–726.
Mangi, S. A., Jamaluddin, N., Wan Ibrahim, M. H., Noridah, M., & Sohu, S. (2017). Utilization of sawdust ash as cement replacement for the concrete production: A review. *Engineering Science and Technology International Research Journal, 1*(3), 11–15.
Mansour, W., & Fayed, S. (2021). Flexural rigidity and ductility of RC beams reinforced with steel and recycled plastic fibers. *Steel and Composite Structures, 41*(3), 317–334.
Mansour, W., Tayeh, B. A., & Tam, L. H. (2022). Finite element analysis of shear performance of UHPFRC-encased steel composite beams: Parametric study. *Engineering Structures, 271*, 114940.
Opiso, E. M., Supremo, R. P., & Perodes, J. R. (2019). Effects of coal fly ash and fine sawdust on the performance of pervious concrete. *Heliyon, 5*(11), e02783.
Oyedepo, O. J., Oluwajana, S. D., & Akande, S. P. (2014). Investigation of properties of concrete using sawdust as partial replacement for sand. *Civil and Environmental Research, 6*(2), 35–42.
Patra, I., Al-Awsi, G. R., Hasan, Y. M., & Almotlaq, S. S. (2022). Mechanical properties of concrete containing recycled aggregate from construction waste. *Sustainable Energy Technologies and Assessments, 53*, 102722.
Shahria Alam, M., Slater, E., & Muntasir Billah, A. H. (2013). Green concrete made with RCA and FRP scrap aggregate: Fresh and hardened properties. *Journal of Materials in Civil Engineering, 25*(12), 1783–1794.
Siddique, R., Singh, M., Mehta, S., & Belarbi, R. (2020). Utilization of treated saw dust in concrete as partial replacement of natural sand. *Journal of Cleaner Production, 261*, 121226.
Ulloa, V. A., García-Taengua, E., Pelufo, M. J., Domingo, A., & Serna, P. (2013). New views on effect of recycled aggregates on concrete compressive strength. *ACI Materials Journal, 110*(6), 687–696.
Vaickelionis, G., & Vaickelioniene, R. (2006). Cement hydration in the presence of wood extractives and pozzolan mineral additives. *Ceramics Silikaty, 50*(2), 115.
Wasim, M., Abadel, A., Bakar, B. H. A., & Alshaikh, I. M. (2022). Future directions for the application of zero carbon concrete in civil engineering—A review. *Case Studies in Construction Materials, 2022*, e01318.
Zapris, A. G., Naoum, M. C., Kytinou, V. K., Sapidis, G. M., & Chalioris, C. E. (2023). Fiber reinforced polymer debonding failure identification using smart materials in strengthened T-shaped reinforced concrete beams. *Polymers, 15*(2), 278.
Zeyad, A., Johari, M. A., Tayeh, B. A., & Alshaikh, I. M. (2019). Influence of palm oil fuel ash on properties of high-strength green concrete. *Scientific Journal of King Faisal University Basic and Applied Sciences, 2019*, 20.

Publisher's Note

Ahmed M. Maglad Associate Professor, Department of Civil Engineering, College of Engineering, Najran University, Najran, Saudi Arabia.

Walid Mansour Assistant Professor, Civil Engineering Department, Faculty of Engineering, Kafrelsheikh University, Kafrelsheikh, 33511, Egypt.

Sabry Fayed Assistant Professor, Civil Engineering Department, Faculty of Engineering, Kafrelsheikh University, Kafrelsheikh, 33511, Egypt.

Bassam A. Tayeh Associate Professor, Civil Engineering Department, Faculty of Engineering, Islamic University of Gaza, Gaza, Palestine.

Ahmed M. Yosri Assistant Professor, Civil Engineering Department, Faculty of Engineering, Delta University for Science and Technology, Belkas, Egypt.

M. Hamad Assistant Professor, Civil Engineering Department, Faculty of Engineering, Delta University for Science and Technology, Belkas, Egypt.